ARCHIVES OF ELECTRICAL ENGINEERING VOL. 73(4), pp. 1123–1135 (2024)

DOI 10.24425/aee.2024.152114

The model of mechanical stress dependence of 2D magnetic permeability of grain-oriented electrical steel sheets adaptable for finite element-based modeling

PAWEŁ RĘKAS [1], ROMAN SZEWCZYK [1]✉, TADEUSZ SZUMIATA [2], MICHAŁ NOWICKI [3]

[1] *Faculty of Mechatronics, Warsaw University of Technology*
Św. Andrzeja Boboli 8, 02-525 Warsaw, Poland

[2] *Faculty of Mechanical Engineering, Department of Physics, Kazimierz Pulaski Radom University*
Stasieckiego 54, 26-600 Radom, Poland

[3] *Department of Mechatronics, Robotics and Digital Manufacturing, Faculty of Mechanics*
Vilnius Gediminas Technical University, Plytinės g. 25, LT-10105 Vilnius, Lithuania
e-mail: {pawel.rekas.dokt/✉ roman.szewczyk}@pw.edu.pl, t.szumiata@urad.edu.pl,
michal.nowicki@vilniustech.lt

(Received: 09.07.2024, revised: 24.11.2024)

Abstract: The paper presents the model of stress dependence of 2D relative magnetic permeability of anisotropic, grain-oriented M120-27s electrical steel suitable for finite element method modeling. The proposed model was developed based on experimental results acquired using the measuring setup with a testing yoke equipped with a Cardan gyroscopic mechanism and hydraulic press. In the presented model, parameters of the tensor description of 2D relative magnetic permeability were chosen during the feature selection process and identified during differential evolution optimization. The good quality of the proposed model was quantitatively confirmed by the R-squared coefficient, which exceeds 0.997 for all plots of the 2D relative magnetic permeability tensor.

Key words: 2D magnetic permeability, electrical steels, grain-oriented anisotropy, magnetoelastic effect

1. Introduction

Due to the possibility of minimization of power loss, grain-oriented, anisotropic electrical steels play a key role as cores of high-efficiency transformers in power systems [1], hydro-generators [2], and high-speed traction motors [3]. It is estimated that the worldwide annual production volume of grain-oriented electrical steel exceeded 6.9 billion USD (in 2022) [4], making this kind of material one of the most important materials for modern industry.

On the other hand, the efficient development of electrical machines utilizing cores made of grain-oriented, anisotropic electrical steels requires the possibility of accurate and efficient modeling of the functional properties of the key machine components. One of the most commonly used methods of such modeling is the finite element method [5]. It should be highlighted that the finite element method enables the modeling of multi-physics interactions [6], such as the influence of mechanical stresses on the operation of electrical machines, such as power transformers or high-speed electrical motors. On the other hand, such modeling requires an accurate model of the mechanical stress dependence of 2D relative magnetic permeability of electrical steel. From the practical point of view, this dependence should be described in the tensor form to enable efficient solving of the ill-posed differential equations describing magnetic and magneto-elastic systems [7] in the finite element method.

The recently developed method of modeling magneto-elastic characteristics of 2D relative magnetic permeability of electrical steels covers the Jiles-Atherton model extension for anisotropic materials [8–11], complex permeability approach [12], using the theory of orientation distribution functions [13] and the concept of co-energy [14]. However, the practical application of these methods for modeling the magneto-elastic characteristics of 2D relative magnetic permeability of electrical steels in the finite element method is sophisticated from a computational point of view. Moreover, it is difficult to calibrate the models to the acquired results of experimental measurements.

The method of modeling proposed in the paper fills the gap. The proposed model can be applied in finite element modeling environment and enables modeling the mechanical stress dependence of 2D relative magnetic permeability for stresses applied in the different directions considering the magnetization easy axis of electrical steel.

2. Method of experimental investigation

The developed method for testing the magnetic properties of M120-27s transformer sheets has been previously described in [15, 16]. The electrical connection diagram and the magnetic circuit of the measurement system are presented in Fig. 1.

The entire measurement is controlled by a computer with software developed in the LabView environment. Signal and data processing are carried out using the DAQ NI-USB 6341 data acquisition and control card. The magnetizing waveform is passed through a Kepco bipolar power supply and applied to the magnetizing coil of the yoke. Measurement of magnetic flux density in the yoke is performed by the LakeShore fluxmeter model 480. The embedded control system is based on a microcontroller that communicates with the computer. It executes commands, which involve precise positioning of the yoke towards and away from the sample and accurate rotation of the yoke.

The computer communicates with an embedded system that controls the stepper motors of the rotator and the electric linear actuator. Based on readings from the limit switches of the linear actuator and the mechanism ensuring constant pressure of the yoke against the sample, the yoke's approach and retraction from the sample are controlled. The measurement cycle involves applying tensile stress to the sample. Subsequently, the entire mechatronic system is homed, and the yoke is rotated to the desired position using the rotator. Next, the yoke is moved towards the sample until the predetermined pressure of the yoke on the sample is achieved, as determined by the mechanism ensuring constant pressure. Upon reaching the predetermined pressure, the

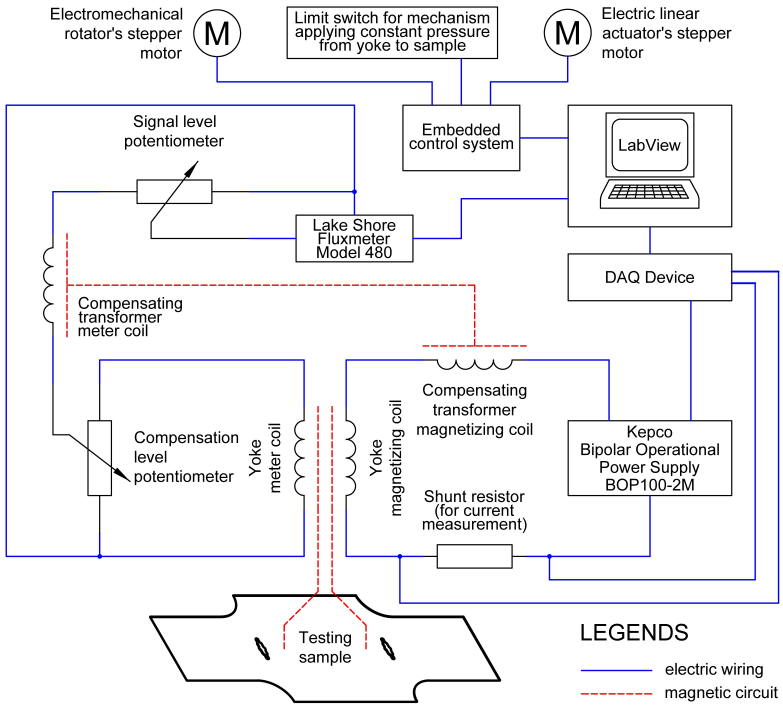

Fig. 1. Schematic block diagram of magnetic circuit and wiring system of measuring setup

yoke is precisely positioned to achieve optimal contact with the sample. This approach ensures measurement repeatability. In the clamped state, magnetic properties are measured. A photograph of the actual measurement setup is shown in Fig. 2.

Since the developed setup investigates the full range of magnetic properties of sheets based on stresses, the angle between the stress direction, rolling direction, and magnetization direction, it is necessary to adjust the position of the yoke relative to the test sample during measurements. This requirement poses a challenge in ensuring optimal clamping to minimize the influence of the magnetic gap on measurements.

This challenge was addressed by using a specially and carefully designed suspension for the measurement yoke. The system has four degrees of freedom. Linear movement along the X-axis allows the yoke to approach and retract from the sample for yoke rotation. Two rotational axes of the yoke – XY and XZ axes – allow for accurate alignment of the yoke relative to the sample to eliminate the formation of a magnetic gap. The fourth degree of freedom – the YZ axis – enables precise rotation of the yoke with a resolution of 1.8° during measurements to examine the sample's magnetic properties over the full 360° range. The kinematic diagram of the yoke suspension is shown in Fig. 3.

The suspension of the measurement yoke was made from non-magnetic materials, as shown in Fig. 3. Positioning is achieved by pressing the yoke against the test sample. The pressure is ensured by a linear drive equipped with a stepper motor. Care was taken to ensure that the pressure was always applied with the same force by using a linear overload clutch.

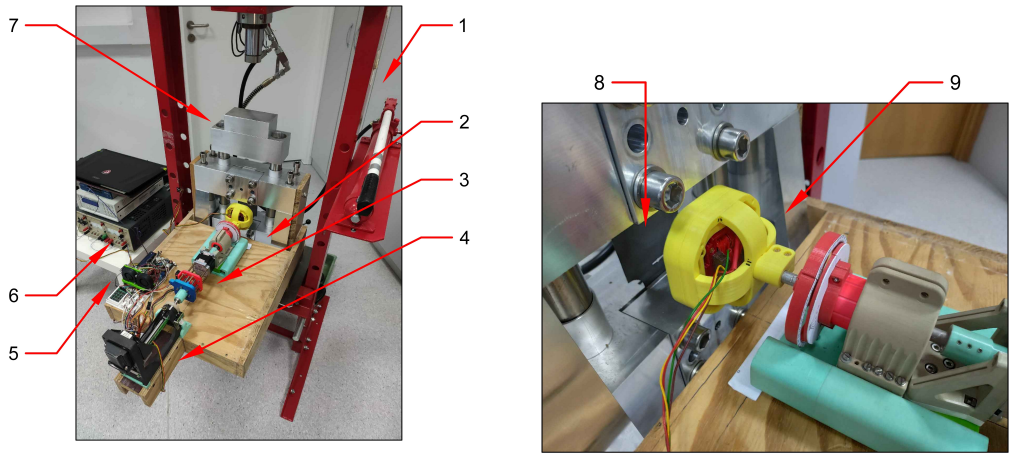

(a) (b)

Fig. 2. Developed automated cushioned yoke system: (a) general view of developed measuring stand; (b) head system during the operation: 1- hydraulic press system, 2 – linear guide with rotator, 3 – cushion system, 4 – linear actuator, 5 – actuators control module, 6 – high power voltage to current converter, 7 – mechanical system with electrical steel sample, 8 – tested sheet sample, 9 – yoke head

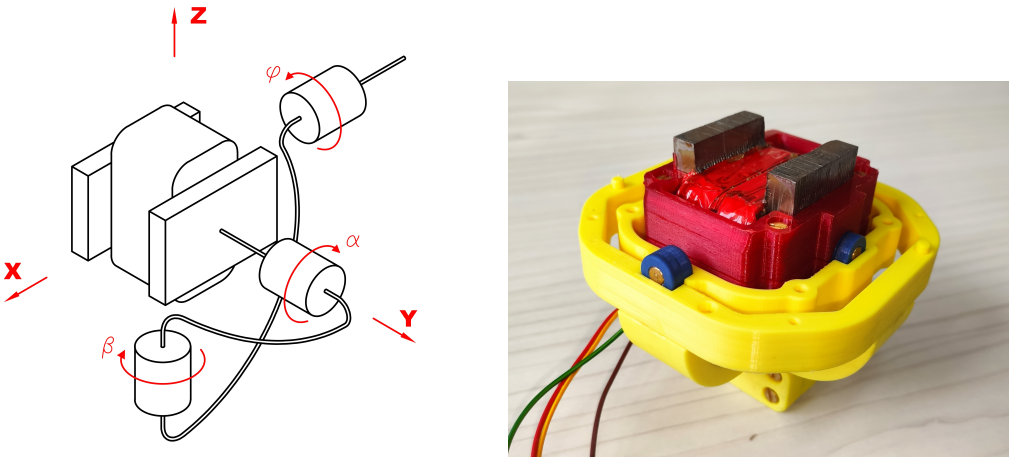

(a) (b)

Fig. 3. The mechanical system of the yoke head with 2D Cardan gyroscopic mechanism: (a) kinetic diagram of automated yoke system head; (b) photograph of the measuring head with Cardan gimbal produced mostly by the 3D printing

3. Proposed model of stress dependence of 2D permeability of electrical steel

Accordingly to the first-assumption, two-domain model utilizing the effective pinning energy [16,17], the generalized, phenomenological description of the mechanical stress σ dependence of the 2D magnetic relative permeability tensor $\hat{\mu}$ of grain-oriented, electrical steel can be given as:

$$\hat{\mu} = \begin{bmatrix} T_1(\gamma,\sigma) & 0 \\ 0 & T_2(\gamma,\sigma) \end{bmatrix} + \begin{bmatrix} T_3(\gamma,\sigma) & 0 \\ 0 & T_4(\gamma,\sigma) \end{bmatrix} \sin^2(\varphi) + \begin{bmatrix} T_5(\gamma,\sigma) & 0 \\ 0 & T_6(\gamma,\sigma) \end{bmatrix} \cos^2(\varphi) + \begin{bmatrix} T_7(\gamma,\sigma) & 0 \\ 0 & T_8(\gamma,\sigma) \end{bmatrix} \sin^6(\varphi), \tag{1}$$

where γ is the angle between the mechanical stresses σ direction and the magnetization easy axis of the grain-oriented, electrical steel sheet, and φ is the angle between the direction of magnetizing field H and the same easy axis.

The proposed model has eight parameters ($T_1(\gamma,\sigma) \ldots T_8(\gamma\sigma)$), which are dependent on each other and lead to ambiguous results of modeling. For this reason, the feature selection [18,19] process was applied on the basis of two following criteria:

- selected parameters should be independent,
- selected parameters should accurately describe the shape of the 2D relative magnetic permeability plot for all tested values of the mechanical stress σ and applied stress angles γ considering the easy axis.

The accuracy indicator F is given as:

$$F = \sum_{i=1}^{n} \left(\mu_{i\text{model}}(\gamma,\sigma,\varphi) - \mu_{i\text{meas}}(\gamma,\sigma,\varphi)\right)^2, \tag{2}$$

where $\mu_{i\text{model}}$ and $\mu_{i\text{meas}}$ are the corresponding results of modeling and measurements, respectively. The value of the accuracy indicator F was determined during differential evolution optimization [20,21] to avoid the influences of possible local minima during the optimization process.

The result of the feature selection process indicated that parameters $T_1(\gamma,\sigma)$, $T_2(\gamma,\sigma)$, $T_4(\gamma,\sigma)$ and $T_7(\gamma,\sigma)$ are sufficient to create the unambiguous and accurate model. As a result of the feature selection process, the model reaches the form:

$$\hat{\mu} = \begin{bmatrix} T_1(\gamma,\sigma) & 0 \\ 0 & T_2(\gamma,\sigma) \end{bmatrix} + \begin{bmatrix} 0 & 0 \\ 0 & T_4(\gamma,\sigma) \end{bmatrix} \sin^2(\varphi) + \begin{bmatrix} 0 & 0 \\ 0 & 0 \end{bmatrix} \cos^2(\varphi) + \begin{bmatrix} T_7(\gamma,\sigma) & 0 \\ 0 & 0 \end{bmatrix} \sin^6(\varphi), \tag{3}$$

which leads to the final form of the proposed model of the 2D magnetic relative permeability tensor:

$$\hat{\mu} = \begin{bmatrix} T_1(\gamma,\sigma) + T_7(\gamma,\sigma)\sin^6(\varphi) & 0 \\ 0 & T_2(\gamma,\sigma) + T_4(\gamma,\sigma)\sin^2(\varphi) \end{bmatrix}. \tag{4}$$

The anisotropic form of the $\hat{\mu}$ tensor, given by Eq. 4, is a simple consequence of the domain walls pinning energy anisotropy [17, 22, 23]. The source of this anisotropy is a strain caused both by the rolling process as well as external load. The physical mechanism of this phenomenon is based both on magnetoelastic interactions in magnetostrictive materials and on the simple geometrical deformations of domain walls pinning centers. The trigonometrical expansion of anisotropic pinning energy imposes only even terms to be non-zero. In the resulting form of the $\hat{\mu}$ tensor (given by Eq. 4), exclusively these trigonometrical terms have been left which are the most crucial in the fitting of experimental data.

It should be highlighted that in anisotropic materials magnetized by the magnetizing field H_ϕ applied at the angle ϕ to the direction of the material's easy axis, the flux density B is not parallel to the vector H_ϕ. As a result, the relative magnetic permeability μ_ϕ observed in the direction ϕ is determined by the projection of a vector $B(H_\phi)$ on the direction of the vector H_ϕ as it is presented in Fig. 4.

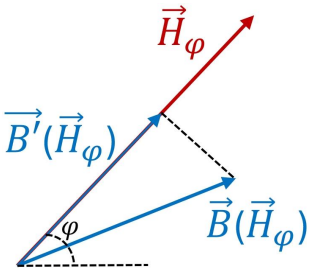

Fig. 4. Magnetizing field H_ϕ inducing flux density vector $B(H_\phi)$ in anisotropic material and its projection on the vector H_ϕ

For the presentation of the relative permeability tensor $\hat{\mu}$ in the form of the polar plot, the value of the relative permeability μ_ϕ at the angle ϕ is calculated on the basis of the dot product determining the projection of a vector $B(H_\phi)$ on the direction of the vector H_ϕ:

$$\mu_\varphi = \mu_0 \frac{\left|\vec{B'}(\vec{H}_\varphi)\right|}{\left|\vec{H}_\varphi\right|} = \mu_0 \frac{\vec{B}(\vec{H}_\varphi) \cdot \vec{H}_\varphi}{\left|\vec{H}_\varphi\right|^2}, \tag{5}$$

where μ_0 is the magnetic constant. Such an approach is judged from the practical point of view due to the fact that in most technical applications, due to coil winding configuration, the flux density B in anisotropic magnetic materials is measured in the direction of the magnetizing field H, as a projection of a vector $B(H_\phi)$ on the direction of the vector H_ϕ.

Considering the fact that $\hat{\mu}$ is the 2D relative magnetic permeability tensor:

$$\vec{B}\left(\vec{H}_\varphi\right) = \hat{\mu}\vec{H}_\varphi. \tag{6}$$

The relative permeability μ_ϕ on the polar plot can be calculated as:

$$\begin{aligned}\mu_\varphi &= \frac{\hat{\mu}\vec{H}_\varphi \cdot \vec{H}_\varphi}{\left|\vec{H}_\varphi\right|^2} \\ &= \frac{\begin{bmatrix} T_1(\gamma,\sigma) + T_7(\gamma,\sigma)\sin^6(\varphi) & 0 \\ 0 & T_2(\gamma,\sigma) + T_4(\gamma,\sigma)\sin^2(\varphi) \end{bmatrix} \begin{bmatrix} \sin\varphi \\ \cos\varphi \end{bmatrix} \cdot H \begin{bmatrix} \sin\varphi \\ \cos\varphi \end{bmatrix} H}{H^2\sin^2\varphi + H^2\cos^2\varphi},\end{aligned} \tag{7}$$

which can be easily simplified to the form:

$$\mu_\varphi = \left[T_1(\gamma,\sigma) + T_7(\gamma,\sigma)\sin^6(\varphi)\right]\cos^2(\varphi) + \left[T_2(\gamma,\sigma) + T_4(\gamma,\sigma)\sin^2(\varphi)\right]\sin^2(\varphi). \tag{8}$$

According to this notation, the results of the application of the proposed model for the modeling of the 2D relative permeability tensor $\hat{\mu}(\gamma,\sigma)$ of M-120-27s grain-oriented electrical steel sheets are presented in Fig. 5. Parameters for modeling a function (γ,σ) were identified by the differential evolution optimization process during the feature selection. The plots of dependence of parameters $T_1(\gamma,\sigma)$, $T_2(\gamma,\sigma)$, $T_4(\gamma,\sigma)$ and $T_7(\gamma,\sigma)$ are presented in Fig. 6.

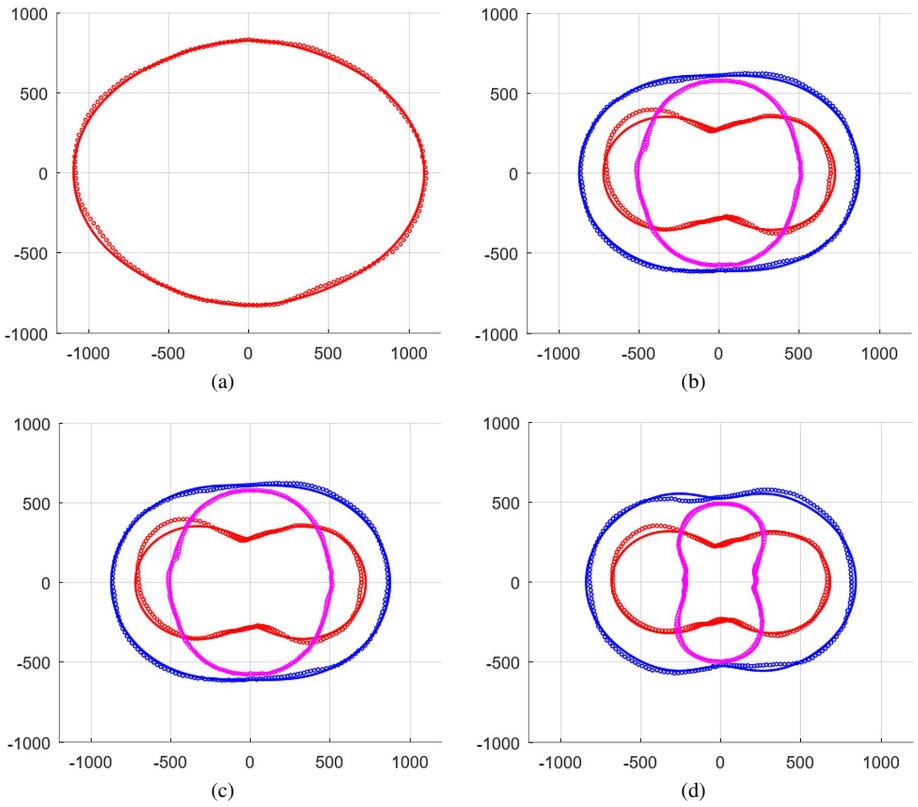

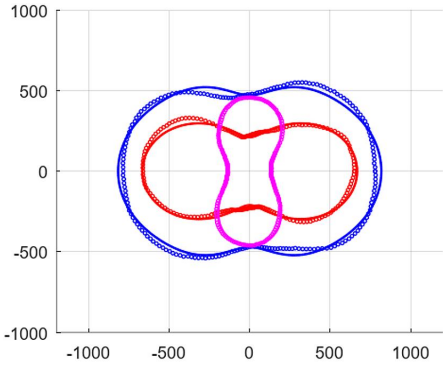

(e)

Fig. 5. The results of measurements (dots) modeling (solid line) the 2D relative permeability tensor $\hat{\mu}(\gamma, \sigma)$ of M-120-27s grain-oriented electrical steel sheets: (a) $\sigma = 0$ MPa; (b) $\sigma = 18.9$ MPa; (c) $\sigma = 44.0$ MPa; (d) $\sigma = 69.1$ MPa; (e) $\sigma = 94.3$ MPa, for different values of angle γ between the magnetization easy axis and the direction of applied stresses (blue: $\gamma = 0$, red: $\gamma = 45°$, magenta: $\gamma = 90°$)

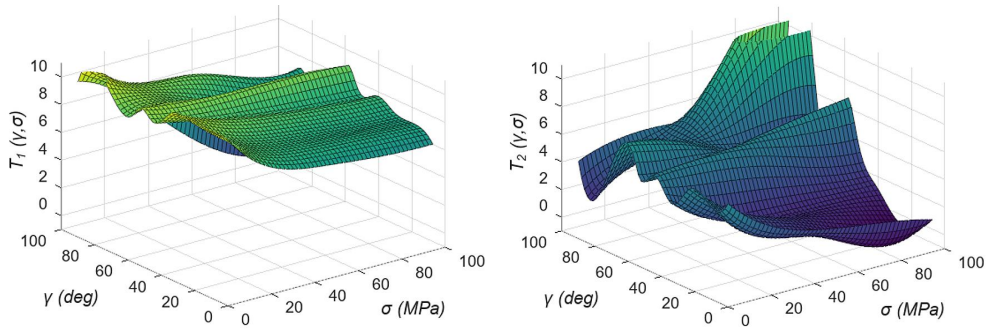

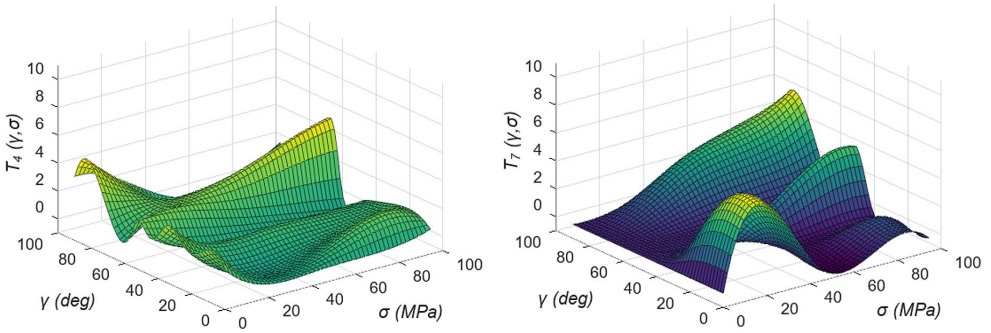

Fig. 6. The results of the model's parameters stress σ and stresses-easy axis angle γ dependence identification using the differential evolution optimization: (a) $T_1(\gamma, \sigma)$; (b) $T_2(\gamma, \sigma)$; (c) $T_4(\gamma, \sigma)$; (d) $T_7(\gamma, \sigma)$

The presented results clearly confirm that the proposed model very well reproduces the 2D relative magnetic permeability tensor $\hat{\mu}(\gamma, \sigma)$ of M-120-27s grain-oriented electrical steel sheets. It should be highlighted that for the moderate range of magnetizing fields (for the amplitude H_m was equal to 750 A/m), both the changes of the shape of the 2D relative magnetic permeability tensor $\hat{\mu}(\gamma, \sigma)$ as well as its values are well described. This quality is quantitatively confirmed by the R-squared coefficient [24,25], which quantifies the part of the variation in experimental results explained by the model. It should be highlighted that the R-squared coefficient exceeds 0.997 for all plots of the 2D relative magnetic permeability tensor $\hat{\mu}(\gamma, \sigma)$ of M-120-27s grain-oriented electrical steel sheets.

However, the physical background of the description of the changes in parameters $T_1(\gamma, \sigma)$, $T_2(\gamma, \sigma)$, $T_4(\gamma, \sigma)$ and $T_7(\gamma, \sigma)$ is difficult to explain. On the other hand, for practical use of the model for finite element method (FEM) modeling, such an explanation is not crucial. As a result, an explanation of the physical background of $T_1(\gamma, \sigma)$, $T_2(\gamma, \sigma)$, $T_4(\gamma, \sigma)$ and $T_7(\gamma, \sigma)$ might be the subject of further investigation.

4. Implementation of the model to FEM software

The proposed model was implemented in the finite element modeling ELMER FEM open-source modeling environment [26,27] as the additional Fortran library. For the test case, the 3-phase transformer was modeled based on the existing T3M 150 solution from Breve Tufvassons Ltd. An elaborated 3D model of the transformer is presented in Fig. 7(a). The dimensions of the core of the transformer are 12.2 cm (length), 15 cm (height), and 5.5 cm (width). The tetrahedral mesh for the model, presented in Fig. 7(b), was generated using open-source NETGEN software, part of the NGsolve toolbox. The number of tetrahedral elements in the core and in each transformer' coil was 1 485 689 and 583 393, respectively.

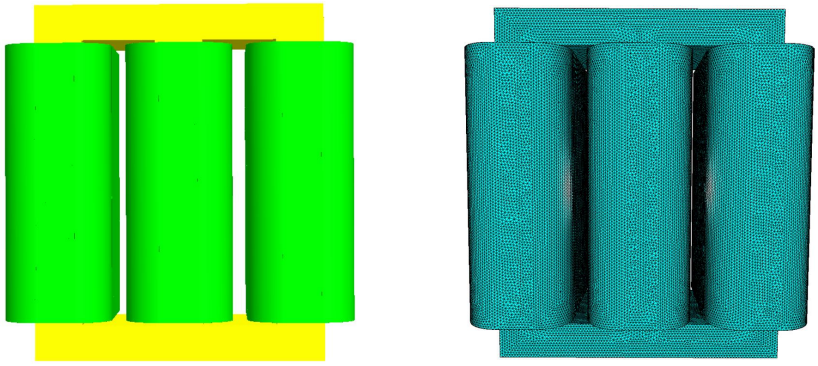

(a) (b)

Fig. 7. The model of the 3-phase transformer: (a) 3D model (yellow – a magnetic core, green – winding); (b) tetrahedral mesh for the model

For the modeling of the mechanical stress distribution in the transformer's core, the 3D model was reduced to a planar system. This was possible due to the system's z-axis symmetry. The results of modeling the mechanical stress σ tensor under the tensile force F applied in the y-axis direction are presented in Fig. 8. Due to the unimportant contribution to the total mechanical stresses, shear stresses τ_{xy} were neglected.

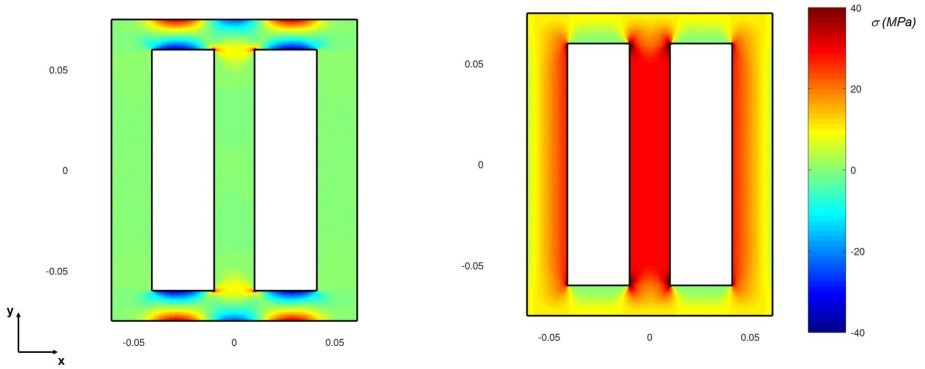

(a) (b)

Fig. 8. Results of modeling the mechanical stress σ distribution in the transformer's core under the tensile force $F = 88$ kN applied in the y-axis direction: (a) σ_{xx}; (b) σ_{yy}

Considering the fact that the 3-phase transformer core is a laminated core, the influence of eddy currents on the magnetic system was neglected. Figure 9 shows the real and imaginary flux density B distribution parts in the modeled core. The modeling was carried out for the sine wave-shaped magnetizing field with an amplitude H_m equal to 750 A/m. The flux density B distribution in the core is presented in Fig. 9 for both its real and imaginary parts.

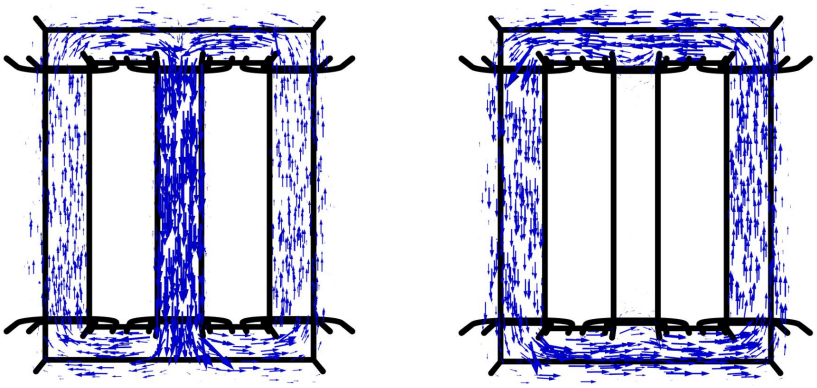

(a) (b)

Fig. 9. Results of modeling the flux density B distribution in the transformer's core under the tensile force $F = 88$ kN applied in the y-axis direction: (a) real part of B; (b) imaginary part of B

The mechanical stress σ dependence of the amplitude of the flux density B is presented in Fig. 10. The plot was elaborated considering the assumption of a sine wave magnetizing field with a given amplitude H_m equal to 750 A/m, and the amplitude of the flux density B was measured in the center of the central middle column of the three-phase transformer. It can be observed that the amplitude of the flux density B is nearly proportional to the magnetic relative permeability of grain-oriented electric steel sheets in the direction of the easy axis and drops from 0.71 T without stresses to 0.21 T for tensile stresses σ equal 94.3 MPa. This phenomenon is caused by the fact that the magnetic permeability of the core's columns plays a key role in determining the functional properties of the three-column frame-shaped transformer's core.

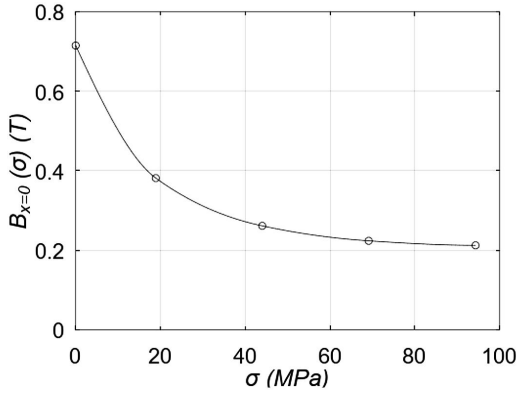

Fig. 10. Mechanical, tensile stress σ dependence of the amplitude of flux density B. The amplitude of the flux density B was measured in the center of the central middle column of the three-phase transformer

5. Conclusions

The presented results confirm that the phenomenological model of the mechanical stress σ dependence of the 2D relative magnetic permeability tensor $\hat{\mu}(\gamma, \sigma)$ efficiently reproduces the results of experimental measurements carried out for anisotropic grain-oriented electrical steel M-120-27s. The quality of the model is confirmed by the determination of the R-squared coefficient, which exceeds 0.997 for the tensile stresses σ up to 94 MPa applied in various directions considering the magnetization easy axis.

The proposed model of the 2D relative magnetic permeability tensor $\hat{\mu}(\gamma, \sigma)$ can be simply applied in finite element modeling environments, such as the open-source ELMER FEM. The results presented in modeling the tensile stress σ dependence of functional properties of a three-phase transformer operating in the current driving mode confirm that the stress dependence of magnetic properties of M-120-27s electrical steel should be considered during the development of electrical devices. It should be highlighted that under the tensile stresses up to 94 MPa, amplitude flux density and corresponding transformer output voltage drop by over 70%. This effect should be considered during the machine development process and observed in technical modeling.

References

[1] Yamaguchi H., Muraki M., Komatsubara M., *Application of CVD method on grain-oriented electrical steel*, Surface and Coatings Technology, vol. 200, no. 10, pp. 3351–3354 (2006), DOI: 10.1016/j.surfcoat.2005.07.051.

[2] Du Y., O'Malley R., Buchely M.F., *Review of magnetic properties and texture evolution in non-oriented electrical steels*, Applied Sciences, vol. 13, no. 10, 6097 (2023), DOI: 10.3390/app13106097.

[3] Gao L., Zeng L., Yang J., Pei R., *Application of grain-oriented electrical steel used in super-high speed electric machines*, AIP Advances, vol. 10, no. 1 (2020), DOI: 10.1063/1.5130151.

[4] *Electrical steel market size, share & growth report*, 2030, Electrical Steel Market Size, Share & Growth Report, 2030, https://www.grandviewresearch.com/industry-analysis/electrical-steel-market, accessed July 9 2024.

[5] Erhunmwun I.D., Ikponmwosa U.B., *Review on Finite Element Method*, Journal of Applied Sciences and Environmental Management, vol. 21, no. 5, 999 (2017), DOI: 10.4314/jasem.v21i5.30.

[6] Kondov I., Sutmann G., *Multiscale Modelling Methods for Applications in Materials Science Cecam Tutorial*, 16–20 September 2013, Forschungszentrum Jülich; Lecture Notes Cecam Tutorial *Multiscale Modelling Methods for Applications in Materials Science*, Organized by Karlsruhe Institute of Technology, Forschungszentrum Jülich, Forschungszentrum Jülich, Institute for Advanced Simulation (IAS), Jülich Supercomputing Centre (JSC), Publ.: Forschungszentrum Jülich GmbH, Zentralbibliothek, Ed. by Ivan Kondov; Godehard Sutmann, Jülich: Forschungszentrum, Zentralbibliothek (2013).

[7] Rubio M.E., Stasyszyn F.A., *Ill-posedness of the mean-field dynamo equations with a linear electromotive force*, Physica D: Nonlinear Phenomena, vol. 430, 133097 (2022), DOI: 10.1016/j.physd.2021.133097.

[8] Jiles D.C., Atherton D.L., *Theory of ferromagnetic hysteresis (invited)*, Journal of Applied Physics, vol. 55, no. 6, pp. 2115–2120 (1984), DOI: 10.1063/1.333582.

[9] Jiles D.C., Atherton D.L., *Theory of ferromagnetic hysteresis*, Journal of Magnetism and Magnetic Materials, vol. 61, no. 1–2, pp. 48–60 (1986), DOI: 10.1016/0304-8853(86)90066-1.

[10] Lihua Z., Jingjing L., Qingxin Y., Jianguo Z., Koh C.-S., *An improved magnetostriction model for electrical steel sheet based on Jiles–Atherton Model*, IEEE Transactions on Magnetics, vol. 56, no. 3, pp. 1–4 (2020), DOI: 10.1109/tmag.2019.2951824.

[11] Raghunathan A., Melikhov Y., Snyder J.E., Jiles D.C., *Generalized form of anhysteretic magnetization function for Jiles–Atherton Theory of hysteresis*, Applied Physics Letters, vol. 95, no. 17 (2009), DOI: 10.1063/1.3249581.

[12] Baghel A.P.S. *et al.*, *An alternative approach to model mechanical stress effects on magnetic hysteresis in electrical steels using complex permeability*, Computational Materials Science, vol. 166, pp. 96–104 (2019), DOI: 10.1016/j.commatsci.2019.03.048.

[13] Tolentino G.C., Leite J.V., Parent G., Batistela N.J., *Implementation of the magnetic anisotropy in 2D finite element method using the theory of orientation distribution functions*, 2020 IEEE 19th Biennial Conference on Electromagnetic Field Computation (CEFC) (2020), DOI: 10.1109/cefc46938.2020.9451381.

[14] Chwastek K., *Anisotropic properties of non-oriented steel sheets*, IET Electric Power Applications, vol. 7, no. 7, pp. 575–579 (2013), DOI: 10.1049/iet-epa.2013.0087.

[15] Rękas P., Nowicki M., Gazda P., Charubin T., Szumiata T., Szewczyk R., *A measuring setup for testing the mechanical stress dependence of magnetic properties of electrical steels*, Journal of Magnetism and Magnetic Materials, vol. 577, 170791 (2023), DOI: 10.1016/j.jmmm.2023.170791.

[16] Szumiata T., Rekas P., Gzik-Szumiata M., Nowicki M., Szewczyk R., *The two-domain model utilizing the effective pinning energy for modeling the strain-dependent magnetic permeability in anisotropic grain-oriented electrical steels*, Materials, vol. 17, no. 2, 369 (2024), DOI: 10.3390/ma17020369.

[17] Rękas P., Szumiata T., Szewczyk R., Gzik-Szumiata M., Nowicki M., *Influence of mechanical stresses noncoaxial with the magnetizing field on the relative magnetic permeability of electrical steel*, IEEE Transactions on Magnetics, vol. 60, iss. 8 (2024), DOI: 10.1109/tmag.2024.3418668.

[18] Büyükkeçeci M., Okur M.C., *A comprehensive review of feature selection and feature selection stability in machine learning*, Gazi University Journal of Science, vol. 36, no. 4, pp. 1506–1520 (2023), DOI: 10.35378/gujs.993763.

[19] Pudjihartono N., Fadason T., Kempa-Liehr A.W., O'Sullivan J.M., *A review of feature selection methods for machine learning-based disease risk prediction*, Frontiers in Bioinformatics, vol. 2 (2022), DOI: 10.3389/fbinf.2022.927312.

[20] Ahmad M.F., Isa N.A., Lim W.H., Ang K.M., *Differential evolution: A recent review based on state-of-the-art works*, Alexandria Engineering Journal, vol. 61, no. 5, pp. 3831–3872 (2022), DOI: 10.1016/j.aej.2021.09.013.

[21] Opara K.R., Arabas J., *Differential evolution: A survey of theoretical analyses*, Swarm and Evolutionary Computation, vol. 44, pp. 546–558 (2019), DOI: 10.1016/j.swevo.2018.06.010.

[22] Krause T.W., Krause A.K., Underhill P.R., Kashefi M., *Modeling magnetization processes in steel under stress using magnetic objects*, Journal of Applied Physics, vol. 131, no. 17 (2022), DOI: 10.1063/5.0088329.

[23] Ito S., Mifune T., Matsuo T., Kaido C., Takahashi Y., Fujiwara K., *Simulation of the stress dependence of hysteresis loss using an energy-based domain model*, AIP Advances, Special Collection: 23rd Soft Magnetic Materials Conference, vol. 8, no. 4, 047501 (2017), DOI: 10.1063/1.4993661.

[24] Nagelkerke N.J., *A note on a general definition of the coefficient of determination*, Biometrika, vol. 78, no. 3, pp. 691–692 (1991), DOI: 10.1093/biomet/78.3.691.

[25] Yin P., Fan X., *Estimating R2 shrinkage in multiple regression: A comparison of different analytical methods*, The Journal of Experimental Education, vol. 69, no. 2, pp. 203–224 (2001), DOI: 10.1080/00220970109600656.

[26] Vencels J., Råback P., Geža V., *EOF-Library: Open-source Elmer Fem and openfoam coupler for electromagnetics and Fluid Dynamics*, SoftwareX, vol. 9, pp. 68–72 (2019), DOI: 10.1016/j.softx.2019.01.007.

[27] Safinowski M., Szudarek M., Szewczyk R., Winiarski W., *Capabilities of an open-source software, Elmer FEM, in finite element analysis of fluid flow*, Recent Advances in Systems, Control and Information Technology, pp. 118–126 (2016), DOI: 10.1007/978-3-319-48923-0_16.